Temperature-dependent transport and $1/f$ noise mechanisms in single-walled carbon nanotube films

Ashkan Behnam,[1,*,†] Amlan Biswas,[2] Gijs Bosman,[1] and Ant Ural[1,*,‡]
[1]*Department of Electrical and Computer Engineering, University of Florida, Gainesville, Florida 32611, USA*
[2]*Department of Physics, University of Florida, Gainesville, Florida 32611, USA*
(Received 27 September 2009; revised manuscript received 8 February 2010; published 5 March 2010)

The temperature dependence of $1/f$ noise and resistivity in single-walled carbon nanotube (CNT) films are studied. We find that as the temperature decreases, resistivity monotonically increases whereas $1/f$ noise amplitude first decreases, then increases, reaching a minimum at around 40 K. At temperatures considerably smaller than 40 K, the temperature dependence of both resistivity and $1/f$ noise amplitude can be explained by three-dimensional Mott variable-range hopping, which is due to localization effects that result in an insulating behavior in CNT films. At higher temperatures, on the other hand, the dependence of resistivity on temperature can be explained by fluctuation-induced tunneling. In this high-temperature regime, we analyze the temperature dependence of the noise amplitude to extract the density of fluctuators as a function of their energy. Our results show a characteristic peak between 0.3 and 0.6 eV that is responsible for the majority of $1/f$ noise. We also find that, due to its correlation with the number of carriers, the noise amplitude is very sensitive to CNT film device dimensions, especially near the percolation threshold where the resistivity increases. These results not only provide fundamental physical insights about transport and $1/f$ noise mechanisms in CNT films at different temperatures but also help assess the suitability of these films for device applications.

DOI: 10.1103/PhysRevB.81.125407 PACS number(s): 73.63.Fg, 72.70.+m

I. INTRODUCTION

Single-walled carbon nanotube (CNT) three-dimensional (3D) films are transparent, conductive, and flexible.[1–3] They also exhibit uniform physical and electronic properties and can be mass produced in a cost effective manner.[1,3] Due to these favorable properties, several promising device applications of CNT films have recently been demonstrated, such as thin-film transistors,[4,5] infrared bolometers,[6] optoelectronic and photovoltaic devices and sensors,[7–10] and chemical sensors.[11,12] For applications such as chemical and optoelectronic sensors, intrinsic noise level is an important figure of merit that determines the detection limit of the device. For both single nanotubes (regardless of their diameter and chirality) and CNT films, low-frequency $1/f$ noise level has been shown to be quite high compared to conventional thin-film metals.[13–15] It is important to determine the source and magnitude of the $1/f$ noise in CNT films not only to better understand the physics involved but also to correctly assess their potential for applications sensitive to noise.

There have been a few studies either on understanding the mechanisms responsible for noise in individual nanotubes[16,17] or on the scaling of $1/f$ noise in CNT networks and films as a function of their dimensions or carrier density.[14,18] It has been shown that for both individual nanotubes and CNT films, current noise spectral density (S_I) obeys the empirical equation,

$$\frac{S_I}{I^2} = \frac{A}{f^\beta} \tag{1}$$

at low frequencies, where I is the current bias, f is the frequency, β is the frequency scaling exponent (close to 1 for $1/f$ noise), and A is the noise amplitude.[19] It has been shown that for individual tubes, A is inversely proportional to the number of carriers in the nanotube and therefore to the length of the tube between the contacts.[20] For CNT films, A has been shown to depend both on device dimensions and resistivity of the film due to the percolative nature of transport.[18]

More information about the nature of the noise sources and their energy distribution in CNT films can be obtained by investigating the temperature dependence of $1/f$ noise. For individual semiconducting nanotubes, a recent study has shown a peak at around 0.4–0.5 eV, which has been related to the traps at the interface between the nanotube and the oxide substrate.[17] However, the temperature dependence of $1/f$ noise in CNT films remains unexplored. Such a study for weakly doped CNT films can be expected to show more interesting results due to the localization effects that result in insulating behavior at low temperatures.[21]

In this paper, we study the temperature dependence of $1/f$ noise in CNT films by fabricating four-point-probe structures and measuring their resistivity and noise amplitude as a function of temperature and frequency. We first analyze the resistivity data to determine the mechanisms that are responsible for electronic transport in CNT films at various temperature ranges. We then interpret our noise data in association with the resistivity results. Our results suggest that at very low temperatures ($T \ll 40$ K), 3D variable-range hopping (VRH) is the dominant mechanism for both resistivity and $1/f$ noise. At temperatures above 40 K, however, the fluctuation-induced tunneling (FIT) model explains the resistivity behavior. In this high-temperature region, we analyze the temperature dependence of the noise amplitude to extract the density of fluctuators as a function of their energy. Finally, we find that the amplitude of $1/f$ noise changes significantly as device length and width shrink, especially in the region that the change in device dimensions results in a change in film resistivity. These results not only provide fundamental physical insights about transport and $1/f$ noise mechanisms in CNT

films but also assist in determining the suitability of these films for applications that need to be reliable over a large temperature window or that are susceptible to noise.

II. EXPERIMENTAL PROCEDURE

CNT films were produced using a vacuum filtration process described in detail previously.[1,22,23] Film thicknesses of ~75 nm that are far above the percolation threshold (which is a few nanometers) were used for this study. Following the deposition, the CNT film was patterned into four-point-probe structures by photolithography or e-beam lithography (depending on the device width) and subsequently etched using an O_2 chemistry in an inductively coupled plasma reactive ion etcher, as described in detail previously.[22,23] Finally, the contact areas on each structure were connected to the sample holder using conductive silver-based epoxy glue and gold wires. Then the sample was inserted into the low-temperature setup which uses a Janis variable-temperature insert to achieve a temperature range from 300 K down to 1.2 K. By using four-point-probe structures, the contribution of contacts to both resistance and noise are eliminated. For noise measurements, a constant current source consisting of a battery and a resistor was used, the voltage fluctuations were then magnified via an ultralow-noise amplifier (BrookDeal, 60 dB gain) and the voltage noise spectral density S_V was measured using an HP 3582 A spectrum analyzer and then converted to S_I. The effects of amplifier and resistance thermal noise sources were subtracted from the measured spectrum by repeating the measurement for a low-noise resistor with the same resistance value as that of the CNT film device.

An optical microscope image of a typical four-point-probe structure fabricated using photolithography is presented in the left inset of Fig. 1 where the device length L and device width W are illustrated. For this study, two sets of CNT film devices have been prepared: The first set (set 1) includes devices with large dimensions well above the percolation threshold (with dimensions $L=1500$ μm and $W=50$ μm, $L=1000$ μm and $W=25$ μm, $L=1000$ μm and $W=50$ μm, and $L=50$ μm and $W=5$ μm). The second set (set 2) includes devices with narrow widths approaching the percolation threshold ($L=50$ μm and W ranging from 0.3 to 2 μm). We have previously demonstrated that the resistivity of CNT films increases significantly for $W<2$ μm since the film gets closer to the percolation threshold.[22]

III. RESULTS AND DISCUSSION

Figure 1 shows the log-log plot of resistivity (ρ) versus temperature (T) for one of the devices in set 1 with $L=1500$ μm and $W=50$ μm (this device will be called D1 from now on). It is clear that ρ increases over 1 order of magnitude as T decreases from 300 to 1.2 K. For CNT films, the temperature dependence of ρ depends strongly on parameters such as the doping of the film, the density and structure of the nanotubes (e.g., diameter and length), and device dimensions.[21,24] For example, while highly doped thick CNT films were found to show metallic behavior with very weak ρ

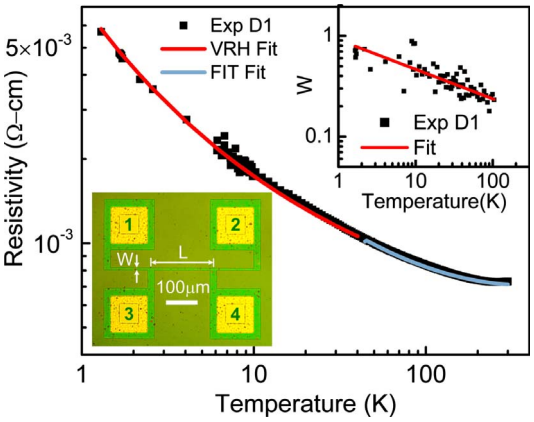

FIG. 1. (Color online) Log-log plot of ρ versus T for device D1. Black squares are experimental data points while red (dark) and blue (light) lines are fits to the experimental results based on the VRH and FIT models, respectively. The right inset is a log-log plot of reduced activation energy (W) versus T for the same device. The solid line in this inset is a power-law fit to the data with an exponent −0.29. The left inset is an optical microscope image of a four-point-probe structure with $L=200$ μm and $W=10$ μm etched out of a CNT film with a thickness of 75 nm. Yellow (light) squares labeled from 1 to 4 are Cr/Pd (10 nm/50 nm) metal pads deposited on top of the film contact areas.

dependence on T, lightly doped or undoped thin CNT films depicted strong localization behavior with close to zero conductance values at very low temperatures.[21,24]

Although the CNT films in our study are not intentionally doped, nitric acid, which is used for purifying the nanotubes, unintentionally dopes the CNT films to some extent. However, as we have previously reported, nanotubes are subsequently dedoped during the processing steps associated with the four-point-probe structure patterning, resulting in weakly doped films.[22,23] The resistivity shown in Fig. 1 for device D1, therefore, depicts insulating behavior due to strong localization of carriers at low temperatures, which can be explained by VRH. The temperature dependence of ρ in the VRH regime can be written as

$$\rho(T) = \rho_0 \exp[(T_0/T)^p], \tag{2}$$

where ρ_0 is a constant, T_0 is the characteristic temperature which is proportional to the energy separation between the available states, and $p=1/(d+1)$ for Mott VRH,[25] where d is the dimensionality of the hopping conduction. As is shown in the right inset of Fig. 1, p can be extracted from a plot of reduced activation energy W, defined as

$$W(T) = -\frac{d \ln[\rho(T)]}{d \ln T}, \tag{3}$$

versus T. The p value (equal to the slope of the fit in this plot) we have extracted is 0.29, which is very close to the theoretical value of 0.25 expected for 3D VRH [i.e., $d=3$ in Eq. (2)]. The slight deviation of p from 0.25 could be either related to a shift from 3D VRH to two-dimensional VRH transport, which is unlikely here due to the 3D structure of the 75-nm-thick CNT film or it could be related to the strong

localization of carriers which causes a transition form Mott VRH to Coulomb gap (CG) VRH. (For CG VRH, the extracted exponent p should have a value close to 0.5.)[21] The latter explanation is more likely in this case, especially as the film is not heavily doped and therefore the intertube coupling could be rather weak in various regions of the film.

The value extracted for T_0 by fitting the experimental data with Eq. (2), as shown in the main panel of Fig. 1, is 39 K. VRH is responsible for transport when $T \ll T_0$. At higher temperatures, FIT can describe the transport in the CNT film, as the conduction paths are formed by very conductive nanotubes in series with resistive tunneling junctions between them.[26,27] The expression for the FIT-controlled resistivity can be written as

$$\rho(T) = C \exp\left(\frac{T_b}{T_s + T}\right), \tag{4}$$

where C is a constant, kT_b reflects the order of magnitude of the barrier energies (where k is the Boltzmann constant) and the T_s to T_b ratio determines the increase in resistivity at lower temperatures. The values of C and T_b can be extracted directly from the data by plotting $\ln(\rho)$ versus $1/T$ (assuming T_s is small) and then T_s can be found from a fit to the data, as shown in the main panel of Fig. 1. From this fit, we get $T_b = 24$ K and $T_s = 14$ K. The values reported for T_b and T_s in the literature vary over a large range[3,28] and the ones extracted here are within that range.[28] T_s is an important parameter here because the FIT model only explains the resistivity results for temperatures that are well above T_s. Therefore, T_s together with T_0 (from the VRH model) suggest that at low temperatures, VRH is the main transport mechanism whereas at high temperatures, FIT begins to dominate. We will show that this is also in agreement with our results on the temperature dependence of $1/f$ noise in CNT films.

The existence of different conduction regimes in CNT films motivates a study on their $1/f$ noise scaling as a function of temperature. An example of the noise current spectral density measured at room temperature for a device in set 1 under 75 μA current bias is shown in the inset of Fig. 2. At this current level, $1/f$ noise is dominant at low frequencies $\sim f < 100$ Hz, obeying Eq. (1) with $\beta = 0.99$ whereas at higher frequencies Nyquist thermal noise, which has a constant current noise spectral density given by $S_I = 4kT/R$, where R is the CNT film resistance, becomes the dominant noise source. In the $1/f$ noise regime, $S_I \propto I^2$ for all of the devices measured.

The main panel of Fig. 2 shows a log-log plot of the noise amplitude A versus T for two devices, namely, D1 (the device for which the resistivity is shown in Fig. 1) and one device in set 2 (with $L = 50$ μm and $W = 0.4$ μm, which will be called device D2). Based on a careful analysis of the noise spectrum at low frequencies, no features other than $1/f$ behavior were detected over the range of measured temperatures (except for slight fluctuations in the exponent β as T varies, as shown in the inset of Fig. 3). Due to the high resistance of D2 at low temperatures, we were able to perform noise measurements only down to 77 K for this device. The temperature-dependent resistivity and noise measurements performed on a few other devices in set 1 and set 2 resulted in similar trends compared to those shown in Figs. 1 and 2 down to the lowest temperatures measured. The temperature dependence of A in Fig. 2 follows the same pattern for both D1 and D2 for $T > 77$ K. However, there is roughly 4 orders of magnitude difference in the absolute value of A in these samples, which will be discussed later when we consider the effect of device dimensions on noise. At high temperatures close to 300 K, A is a weak function of T, however, as T decreases down to 77 K, A starts to decrease for both D1 and D2. The value of A for D1 reaches a minimum at around 40 K and then starts to increase significantly at lower temperatures. This trend is strikingly different from the one that

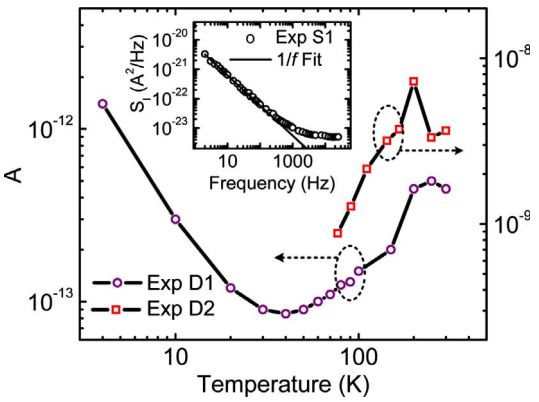

FIG. 2. (Color online) Log-log plot of A versus T for devices D1 (left y axis) and D2 (right y axis). Due to the high resistance of D2 at low temperatures, noise measurements could be performed only down to 77 K for this device. A power-law fit to the three leftmost D1 data points yields an exponent of 1.53. The black lines are drawn as a guide for the eyes. The inset is a log-log plot of current noise spectral density (S_I) versus f for a device in set 1 with $L = 1000$ μm and $W = 50$ μm (open circles), demonstrating the $1/f$-type behavior at low frequencies and saturation of the noise at high frequencies. The black line in this inset is a fit to the low-frequency regime with a slope β of 0.99.

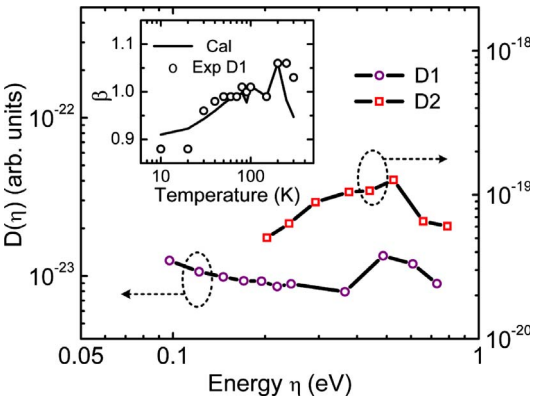

FIG. 3. (Color online) Log-log plot of $D(\eta)$ (arbitrary units) versus η for devices D1 and D2 directly obtained from A versus T results in Fig. 2. The black lines are drawn as a guide for the eyes. The inset is a linear-log plot of β versus T for D1 either experimentally obtained (open circles) or directly calculated from A versus T results in Fig. 2 at 1 Hz.

has been recently observed for individual semiconducting nanotubes,[17] where A continuously decreases as T goes down to 4 K. Due to the insulating behavior of the CNT film at low temperatures (A and ρ both increase significantly when T decreases), the noise behavior might be determined by two separate mechanisms at high and low temperatures. For D1 at $T \ll 40$ K, A exhibits a power-law dependence on T in the form $A \propto T^{-\nu}$ with $\nu=1.53$. It has been suggested that for Mott VRH systems in which A increases as T decreases, a power-law-based relationship with an exponent close to 1.5 exists between A and T.[29] The exponent v extracted from our data is very close to this value. Another interesting feature is the position of the noise minimum in the A vs T curve for D1, which is ~40 K. This temperature is very close to the T_0 value in the VRH model extracted from the ρ vs T data. These observations imply that VRH theory applies to the temperature dependence of both resistivity and noise in our CNT films at low temperatures ($T \ll 40$ K).

The T dependence of A at temperatures above the VRH regime can provide further information about the energy distribution of the fluctuators. More specifically, Dutta and colleagues have suggested that for an inhomogeneous system with random fluctuations, if the energy distribution is broad compared to kT, the relationship between $D(\eta)$, density of fluctuation states, and A can be written in the form[30]

$$D(\eta) \propto \frac{A(T)}{T}, \tag{5}$$

where $\eta=-kT\ln(2\pi f\tau_0)$, and τ_0 is a characteristic "attempt time" with a value inverse of phonon frequency. For most materials, $10^{-14} < \tau_0 < 10^{-11}$ s (Ref. 31) but the value of η is not very sensitive to the absolute value of τ_0.

The main panel of Fig. 3 shows $D(\eta)$ versus η for D1 and D2, based on Eq. (5) with $\tau_0=10^{-13}$ s. This value of τ_0 is chosen to provide the best fit of Eq. (6) to the β values extracted experimentally, as explained below. The similarity in the dependence of A on temperature for the two devices results in a similarity in the dependence of D on η. As can be seen, both curves show broad peaks in the range 0.3–0.6 eV. These peaks are broad enough to satisfy the assumptions made in writing Eq. (5) and they are responsible for most of the noise at high temperatures.[30] As mentioned before, similar peaks have also been observed for individual semiconducting tubes.[17] Based on the energy range of the peaks, sources of noise such as electronic excitations within the tubes or structural fluctuation of the defects within the CNT lattice have been ruled out.[17] For CNT films, due to the presence of the tube-tube junctions, the picture is even more complicated. However, a possible source of the noise could be fluctuation within or at the surface of the SiO_2 substrate underneath the nanotubes.[17] In fact, it has been shown that removing the oxide underneath the tubes can improve (reduce) their noise amplitude up to an order of magnitude.[32,33] Therefore, similar to the individual semiconducting nanotube case, a significant portion of the noise observed at room temperature in CNT films can also be related to the fluctuation of trapped charges in the oxide.

Based on Dutta *et al.*,[30] there should also be a relationship between the frequency-scaling exponent β and the dependence of the voltage noise spectral density S_v on temperature in the form

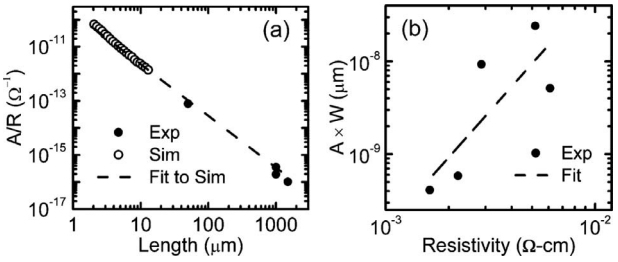

FIG. 4. (a) Log-log plot of measured (filled circles) and simulated (open circles) A/R versus L. Measured values are for devices in set 1. The extracted critical exponent from the dashed line power-law fit (i.e., $A/R \propto L^{-\kappa}$) to the simulation dataset is 1.9. (b) Log-log plot of $A \times W$ versus ρ experimentally measured for devices in set 2 (with $L=50$ μm and $W=0.3$, 0.4, 0.7, 1, and 2 μm). The critical exponent extracted from a fit (in the form $A \times W \propto \rho^{\delta}$) to the results is 2.5.

$$\beta \propto 1 - \frac{1}{\ln(2\pi f\tau_0)}\left[\frac{\partial \ln S_v}{\partial \ln T} - 1\right]. \tag{6}$$

In this equation, β varies as a function of both T and f and therefore its dependence on T can be calculated at various frequencies. At a fixed frequency of $f=1$ Hz, Eq. (6) simplifies to

$$\beta \propto 1 - \frac{1}{\ln(2\pi\tau_0)}\left[\frac{\partial \ln A}{\partial \ln T} - 1\right]. \tag{7}$$

In order to check the accuracy of Eq. (5) for CNT films, the inset in Fig. 3 compares the values of β as a function of T that are extracted from the experimental results and calculated from Eq. (7). The agreement between the two sets is very good for $T > 40$ K (above the VRH regime) and so the relationship between the energy distribution of fluctuations and the temperature scaling of the noise amplitude stated in Eq. (5) is correctly established. Furthermore, for other low-frequency values in the range $0.1 < f < 10$ Hz, there is no significant change in the absolute value of β and its temperature dependence with frequency, and therefore there is good agreement between the experimentally extracted β values and those based on Eq. (6).

As mentioned before, the value of A at room temperature is about 4 orders of magnitude larger for device D2 compared to D1 (see Fig. 2). This difference is due to two reasons: first, the dimensions of D2 ($L=50$ μm and $W=0.4$ μm) are significantly smaller compared to those of D1 ($L=1500$ μm and $W=50$ μm). It has been shown that for CNT films, A is almost inversely proportional to the total number of carriers (N) and hence inversely proportional to both L and W in the region that film resistivity is constant (i.e., well above the percolation threshold).[14,18] As a result, the large difference between the dimensions of the two devices can partially explain the difference in their A values. Figure 4(a) shows the measured values of the noise amplitude normalized to resistance (A/R) at room temperature versus device length (L) for four devices in set 1. Also shown in

this figure are our Monte Carlo simulation results, described in detail previously.[18] The critical exponent extracted from the power-law fit (i.e., $A/R \propto L^{-\kappa}$) to the simulation dataset is 1.9, which is very close to the theoretical value of $\kappa=2$.[14] The decrease in the noise amplitude with device length is consistent with Hooge's classical empirical law,[19] where the $1/f$ noise amplitude A varies inversely with the number of charge carriers N in the device, i.e., $A \propto 1/N$.[14] However, since $R \propto L$ and $N \propto L$, A/R is expected to scale as $A/R \propto L^{-2}$. The experimental data is in very good agreement with the simulation results and the expected $A/R \propto L^{-2}$ dependence.

The second reason for the huge difference in the A values between D1 and D2 is the nonconstant resistivity. The device width W of D2 is very close to percolation threshold and hence its resistivity is much higher compared to D1. The increase in ρ results in a further increase in A, i.e., A dependence on W becomes significantly stronger than an inverse relationship. To better demonstrate the relationship between A and ρ, we have measured A for the devices in set 2 with various widths, and the results are plotted as $A \times W$ versus ρ in Fig. 4(b). If A is inversely proportional to W, $A \times W$ should remain constant as W and hence ρ changes. However, as can be seen in this figure, $A \times W$ depends strongly on ρ, following a power-law relationship with ρ in the form $A \times W \propto \rho^{\delta}$, where δ is extracted to be 2.5. This strong A-ρ dependence is due to the percolative nature of the transport in CNT films, as recently predicted by our computational study of percolation scaling of $1/f$ noise in CNT films.[18] Based on the above discussion, both the dimensions of the device and the resistivity of the film are responsible for the large differences observed in the noise levels of our samples.

IV. CONCLUSIONS

In summary, we have experimentally studied the temperature dependence of resistivity and $1/f$ noise in CNT films. Our results advocate the existence of two different transport regimes for both noise and resistivity. In particular, at temperatures considerably smaller than 40 K, the temperature dependence of both ρ and the noise amplitude A can be explained by 3D Mott variable-range hopping. At higher temperatures, on the other hand, the dependence of ρ on T can be explained by the fluctuation-induced tunneling model. The noise amplitude A exhibits a minimum at around 40 K and then starts to increase with increasing T. In this high-temperature regime, the density of fluctuators as a function of energy, extracted from the T dependence of A, depicts a peak at around 0.3–0.6 eV. The fluctuations within or at the surface of the SiO_2 substrate underneath the CNT film could be the source of this peak and therefore the dominant source of the noise at high temperatures. Our study also shows that A is very sensitive to the dimensions of the CNT film device, due to its correlation with the number of carriers in the system, specially near the percolation threshold. These results not only provide physical insights into charge transport and fluctuations in CNT films as a function of temperature but also illustrate noise scaling trends with device dimensions due to percolation effects.

ACKNOWLEDGMENTS

This work was funded in part by the Semiconductor Research Corporation. A. Biswas acknowledges the support of the U.S. National Science Foundation under Grant No. DMR 0804452. The authors would like to thank Zhuangchun Wu and Andrew Rinzler for providing nanotube films.

*Author to whom correspondence should be addressed.
†abehnam@ufl.edu
‡antural@ufl.edu

[1] Z. Wu, Z. Chen, X. Du, J. Logan, J. Sippel, M. Nikolou, K. Kamaras, J. Reynolds, D. Tanner, A. Hebard, and A. Rinzler, Science **305**, 1273 (2004).
[2] Y. X. Zhou, L. B. Hu, and G. Grüner, Appl. Phys. Lett. **88**, 123109 (2006).
[3] E. Bekyarova, M. E. Itkis, N. Cabrera, B. Zhao, A. P. Yu, J. B. Gao, and R. C. Haddon, J. Am. Chem. Soc. **127**, 5990 (2005).
[4] R. Seidel, A. P. Graham, E. Unger, G. S. Duesberg, M. Liebau, W. Steinhoegl, F. Kreupl, and W. Hoenlein, Nano Lett. **4**, 831 (2004).
[5] C. Kocabas, N. Pimparkar, O. Yesilyurt, S. J. Kang, M. A. Alam, and J. A. Rogers, Nano Lett. **7**, 1195 (2007).
[6] M. E. Itkis, F. Borondics, A. Yu, and R. C. Haddon, Science **312**, 413 (2006).
[7] D. Zhang, K. Ryu, X. Liu, E. Polikarpov, J. Ly, M. E. Tompson, and C. Zhou, Nano Lett. **6**, 1880 (2006).
[8] A. Behnam, J. Johnson, Y. Choi, L. Noriega, M. G. Ertosun, Z. Wu, A. G. Rinzler, P. Kapur, K. C. Saraswat, and A. Ural, J. Appl. Phys. **103**, 114315 (2008).
[9] Y. Jia, J. Wei, K. Wang, A. Cao, Q. Shu, X. Gui, Y. Zhu, D. Zhuang, G. Zhang, B. Ma, L. Wang, W. Liu, Z. Wang, J. Luo, and D. Wu, Adv. Mater. (Weinheim, Ger.) **20**, 4594 (2008).
[10] Z. Li, V. P. Kunets, V. Saini, Y. Xu, E. Dervishi, G. J. Salamo, A. R. Biris, and A. S. Biris, ACS Nano **3**, 1407 (2009).
[11] L. Valentini, I. Armentano, J. M. Kenny, C. Cantalini, L. Lozzi, and S. Santucci, Appl. Phys. Lett. **82**, 961 (2003).
[12] E. S. Snow, F. K. Perkins, E. J. Houser, S. C. Badescu, and T. L. Reinecke, Science **307**, 1942 (2005).
[13] P. G. Collins, M. S. Fuhrer, and A. Zettl, Appl. Phys. Lett. **76**, 894 (2000).
[14] E. S. Snow, J. P. Novak, M. D. Lay, and F. K. Perkins, Appl. Phys. Lett. **85**, 4172 (2004).
[15] S. Soliveres, J. Gyani, C. Delseny, A. Hoffmann, and F. Pascal, Appl. Phys. Lett. **90**, 082107 (2007).
[16] S. Reza, Q. T. Huynh, G. Bosman, J. S. Oakley, and A. G. Rinzler, J. Appl. Phys. **100**, 094318 (2006).
[17] D. Tobias, M. Ishigami, A. Tselev, P. Barbara, E. D. Williams, C. J. Lobb, and M. S. Fuhrer, Phys. Rev. B **77**, 033407 (2008).
[18] A. Behnam, G. Bosman, and A. Ural, Phys. Rev. B **78**, 085431 (2008).
[19] F. N. Hooge, Phys. Lett. A **29**, 139 (1969).

[20] Y. M. Lin, J. Appenzeller, J. Knoch, Z. Chen, and P. Avouris, Nano Lett. **6**, 930 (2006).
[21] J. Vavro, J. M. Kikkawa, and J. E. Fischer, Phys. Rev. B **71**, 155410 (2005).
[22] A. Behnam, L. Noriega, Y. Choi, Z. Wu, A. G. Rinzler, and A. Ural, Appl. Phys. Lett. **89**, 093107 (2006).
[23] A. Behnam, Y. Choi, L. Noriega, Z. Wu, I. Kravchenko, A. G. Rinzler, and A. Ural, J. Vac. Sci. Technol. B **25**, 348 (2007).
[24] V. Skakalova, A. B. Kaiser, Y.-S. Woo, and S. Roth, Phys. Rev. B **74**, 085403 (2006).
[25] N. F. Mott, *Metal-Insulator Transitions*, 2nd ed. (Taylor & Francis, London, 1990).
[26] M. S. Fuhrer, J. Nygard, L. Shioh, M. Forero, Y. G. Yoon, M. S. C. Mazzoni, H. J. Choi, J. Ihm, S. G. Louie, A. Zettl, and P. L. McEuen, Science **288**, 494 (2000).
[27] A. B. Kaiser, Rep. Prog. Phys. **64**, 1 (2001).
[28] T. M. Barnes, J. L. Blackburn, J. van de Lagemaat, T. J. Coutts, and M. J. Heben, ACS Nano **2**, 1968 (2008).
[29] V. I. Kozub, Solid State Commun. **97**, 843 (1996).
[30] P. Dutta, P. Dimon, and P. M. Horn, Phys. Rev. Lett. **43**, 646 (1979).
[31] A. Kolek, A. W. Stadler, P. Ptak, Z. Zawiślak, K. Mleczko, P. Szalański, and D. Żak, J. Appl. Phys. **102**, 103718 (2007).
[32] Y. M. Lin, J. C. Tsang, M. Freitag, and P. Avouris, Nanotechnology **18**, 295202 (2007).
[33] V. K. Sangwan, V. W. Ballarotto, M. S. Fuhrer, and E. D. Williams, Appl. Phys. Lett. **93**, 113112 (2008).